10

Image Fusion Based on Muti-directional Multiscale Analysis and Immune Optimization

Fang Liu, Jing Bai, Shuang Wang, Biao Hou and Licheng Jiao
Key Laboratory of Intelligent Perception and Image Understanding of Ministry of Education of China,
Institute of Intelligent Information Processing Xidian University, Xi'an, P.R. China

1. Introduction

Image fusion is a process by combining two or more source images from different modalities or instruments into a single image with more information. The successful fusion is of great importance in many applications, such as military, remote sensing, computer vision and medical imaging, et al. Image fusion can be performed at signal, pixel, feature and symbol levels depending on the representation format at which image information is processed. The pixel-level image fusion can provide the fine information by fusing the pixels of the source images and the fused images. In this chapter, we only consider the fusion technique on pixel-level. To the pixel-level fusion, some generic requirements can be imposed on the fused on the fusion results (Rockinger, O., 1996):

a. The fused image should preserve all relevant information contained in the source images as closely as possible;
b. The fused process should not introduce any artifacts or inconsistencies, which can distract or mislead the human observer, or any subsequent image processing steps;
c. In the fused image, irrelevant features and noise should be suppressed to a maximum extent.

The visible light sensor and the infrared sensor are in common use sensors acting on different bands. The infrared imaging sensor is sensitive to the radiation of object scene, but not to the brightness change of scene. The visible light imaging sensor is sensitive and decided by the reflectivity and the shadow of the object sensor and has the higher contrast degree, but independent to the heat contrast. The image features of the two kinds of sensors have the different gray values and have the complement information. The fusion of the infrared images and the low visible light images can be in favor of integrating the good object denote character of the infrared images and the clear scene information of the visible light images.

Panchromatic (PAN) images of high spatial resolution can provide detailed geometric information, such as shapes features, and structures of objects of the earth's surface. While multispectral(MS) images with usually lower resolution are used to obtain spectral information necessary for environmental applications. The different objects within images of high spectral resolution are easily identified. Data fusion methods aim to obtain the images with high spatial and spectral resolution, simultaneously. The PAN and MS remote sensing

image fusion is different in military missions or computer-aided quality control. The specificity is to preserve the spectral information for subsequent classification of ground cover. The classical fusion methods are principle component analysis (PCA), intensity-hue-saturation (IHS) transform, etc. In recent years, with the development of wavelet transform (WT) theory and multiresolution analysis, two-dimensional separable wavelets have been widely used in image fusion and have achieved good results(Nunez, J., 1999; Gonzalez-Audicana. M., 2004; Wang, Z. J., 2005). Thus, the fusion algorithms mentioned above can hardly make it by themselves. They usually cause some characteristic degradation, spectral loss, or color distortion. The WT can preserve spectral information efficiently but cannot express spatial characteristics well. Furthermore, the isotropic wavelets are scant of shift-invariance and multidirectionality and fail to provide an optimal expression of highly anisotropic edges and contours in image.

Image decomposition is an important link of image fusion and affects the information extraction quality, even the whole fusion quality. In recent years, along with the development and application to express local signal makes wavelet a candidate in multisensor image fusion. However, wavelet bases are isotropy and of limited directions and fail to represent high anisotropic edges and contours in images well. The MGA emerges, which comes form wavelet, but beyond it. The MGA can take full advantage of the geometric regularity of image intrinsic structures and obtain the asymptotic optimal representation. As an MAG tool, the contourlet transform (CT) has the characteristics of localization, mulitdirection, and anisotropy (Do, M. N., 2005). The CT can give the asymptotic optimal representation of contours and has been applied in image fusion effectively. However, the CT is lack of shift-invariance and results in artifacts along the edges to some extend. The nonsubsampled contourlet transform (NSCT) is in virtue the nonsubsampled filter banks to meet the shift-invariance(da Cunha, 2006). Therefore, the NSCT is more suitable for image fusion, which is explained in section II together with the immune clonal selection (ICS) optimization algorithm.

Considering of the characteristics of low visible light images and infrared images and combining with the human visual system, a novel image fusion technique is presented in section III. The fusion technique is based on ICS in the natural immune selection and the NSCT. The NSCT can give the asymptotic optimal representation of the edges and contours in image by virtue of the characteristics of good multiresolution, shift-invariance and multi-directionality. And then the ICS is introduced into the NSCT domain to optimize the fusing weights adaptively. Numerical tests show that this algorithm provides improvements both in visual effects and quantitative analysis. And the fused images hold more edge and texture information and have stronger contrast and definition.

The fusion of multispectral and panchromatic remote sensing images is discussed in section IV. An NSCT-based panchromatic and multispectral image fusion method is presented after analyzing the basic principles of remote sensing image system and fusion purpose. An intensity component addition strategy based on LHS transform is introduced into NSCT domain to preserve spatial resolution and color content. Experiments show that the fusion method proposed can improve spatial resolution and keep spectral information simultaneously.

A novel image fusion scheme is presented based on multiscale decomposition and multiwavelet transform (MWT) in section V. First, contrast pyramid (CP) decomposition is used to each level of each original image. Then, each image are decomposed by WT.

Furthermore, a kind of evolution computation method-ICS algorithm is introduced to optimize the fusion coefficients for better fusion products. Applying this technique to fusion of multisenor images, simulation results clearly demonstrate the superiority of this new approach. Fusion performance is evaluated through subjective inspection, as well as objective performance measurements. Experimental results show that the fusion scheme is effective and the fused images are more suitable for further human visual or machine perception.

2. NSCT and ICS

2.1 Contourlet transform and NSCT

Do and Vetterli proposed a "true" 2-D transform called contourlet transform, which is based on nonsubsampled filter banks and provides an efficient directional multiresolution image representation. However, because of downsampling and upsampling, CT lacks shift-invariance and results in artifacts. In order to get rid of the frequency aliasing of contourlets and enhance directional selectivity and shift-invariance, nonsubsampled contourlet transform based on nonsubsampled pyramid decomposition and nonsubsampled filter banks (NSFB) is proposed (Jianping, Zhou, 2005). The NSCT provides not only mulitresolution analysis but also geometric and directional representation.

Multiscale decomposition step of the NSCT is realized by shift-invariant filter banks satisfying Bezout identical equation (perfect reconstruction (PR)), not LP of CT. Because of no downsampling in pyramid decomposition, there is no frequency aliasing in low-pass subband, even the band width is larger than π/2. Hence, the NSCT has better frequency characteristic than CT. The two-level NSCT decomposition is shown in Figure 1.

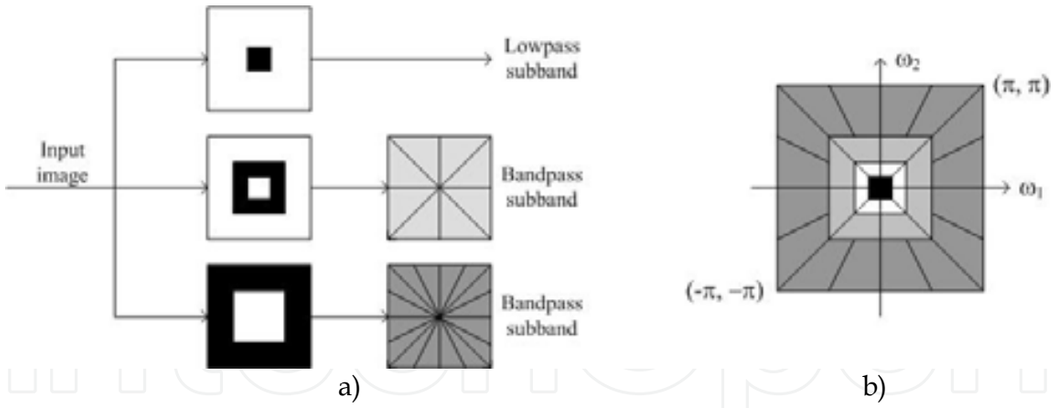

Fig. 1. Two-level NSCT decomposition. (a) NSCT structure that implements the NSCT (b) Frequency partitioning obtained with the proposed structure

The core of the NSCT is the nonseparable two-channel NSFB. It is easier and more flexible to design the needed filter banks that lead to an NSCT with better frequency selectivity and regularity when compared to the corresponding CT. Based on mapping approach and ladder structure fast implementation, the NSCT frame elements are regular and symmetric, and the frame is close to a tight frame. The multiresolution decomposition of NSCT can be realized by nonsubsampled pyramid (NSP), which can reach the subband decomposition structure similar to LP. On j-th decomposition, the desired bandpass support of the low-

pass is $[-\pi/2^j, \pi/2^j]^2$. And then the corresponding band-pass support of the high-pass is the complement set of the low-pass, that is $[-\pi/2^{j-1}, \pi/2^{j-1}]^2 \setminus [-\pi/2^j, \pi/2^j]^2$. The filters of subsequent scales can be acquired through upsampling that of the first stage, which gives the mulitscale property without the need of additional filters desigh. From the computation complexity, on bandpass image is produced at each stage resulting in $J+1$ redundancy. By contrast, the corresponding NSWT produces three directional images at each stage and resulting in $3J+1$ redundancy.

The NSFB is built form a lowpass analysis filter $H_0(z)$ and $H_1(z) = 1 - H_0(z)$. The corresponding synthesis filter $G_0(z) = G_1(z) = 1$. The perfect reconstruction (PR) condition is given as

$$H_0(z)G_0(z) + H_1(z)G_1(z) = 1 \tag{1}$$

2.2 ICS optimization

As a novel artificial intelligent optimization technique, the artificial immune system (AIS) aim at using ideas gleaned from immunology in order to develop systems capable of performing different tasks in various areas of research. The clonal selection functioning of the immune system can be interpreted as a remarkable microcosm of Charles Darwin's law of evolution, with the three major principles of diversity, variation and natural selection.

The clonal selection algorithm is used by the natural immune system to define the basic features of an immune response to an antigenic stimulus (De Castro, L. N. 2000). The main features of the clonal selection theory are: generation of new random genetic changes subsequently expressed as diverse antibody patterns by a form of accelerated somatic mutation; phenotypic restriction and retention of one pattern to one differentiated cell (clone); proliferation and differentiation on contact of cells with antigens. It establishes the idea that only those cells that recognize the antigens are selected to proliferate. The selected cells are subject to an affinity maturation process, which improves their affinity to the selective antigens. Random changes are introduced and will lead to an increase in the affinity of the antibody. It is these high-affinity variants which are then selected to enter the pool of memory cells. Those cells with low affinity receptors must be efficiently eliminated become anergic or be edited, so that they do not significantly contribute to the pool of memory cells.

Evolutionary strategy (ES) is an optimization technique based on group, which considers the feasible solutions as the group and as the operation object. The individual in the group is defined as a real value vector $Y = (y_0, y_1, \cdots, y_n)$, which measures the advantage and disadvantage by the fitness function. The optimization object is to search an optimal individual $Y^* = (y_0^*, y_1^*, \cdots, y_n^*)$ with the largest fitness $Fit(f^*)$. The basic process of the ES is as follows:

a. Produce initial parent-off springs $\{Y_i, i = , \ 1,2,\cdots,\mu\}$ where μ is the number of individuals and uniform distribution on $[0,1]$.

b. Aberrance: Producing subgroup individuals $\{Y_i^j = Y_i + N(0,\delta_j^2)\}$, where $i = 1,2,\cdots,\mu$, $j = 1,2,\cdots,\lambda$. And $N(0,\delta_j^2)$ denotes the Gaussian noise with mean 0 and variance δ^2, where the variance can be fixed or change adaptively.

c. Reselection: we can adopt the fixed or random selection methods. In this chapter, we adopt the fixed selection and avoid loosing in the local optimal, which means selecting the optimal μ individuals from the $\mu + \mu\lambda$ individuals and composing new parent group.
d. Repeating the (b) and (c) steps until the fitness function satisfy the end requirement or the iterated run time reach the maximum permissible run time. The terminal resolution is the optimal individual of the last generation group.

The definition of antigen, antibody, and antigen is as follows:

Antigen: it denotes the question and the corresponding constraint and like to the fitness function of evolution algorithm. For detail, it is the function of the object function $f(x)$ and denoted as $g(f(x))$, which is the important weighted index of starting factor and the algorithm performance in the artificial immune system However, the determination of the antigen g usually needs considering the intrinsic characteristics of the question, that is to say, needs to combine with the prior knowledge. Generally, for simple disposal and under the unspecified case, we adopt $g(x) = f(x)$.

Antibody: It denotes the candidate solutions of the question in the artificial immune system, which is the same to the evolution algorithm.

Antigen—antibody affinity, Avidity: reflects the whole adhesion between the molecular antibody and antigen. In the artificial immune system, the avidity denotes the object function values or the fitness of the candidate solutions to question.

a. **Clonal oprating T_c^C**

The essence of the clonal operating is that the producing of new sub-group around candidate solutions based on the values of the affinity during the immune process. The colnal process enlarges the search range. The definition of clonal is as follows:

$$\begin{aligned} A'(k) &= [A_1'(k)\ \ A_2'(k)\ \ \cdots\ \ A_n'(k)] = \mathrm{T}_\mathrm{c}^\mathrm{C}(A(k)) \\ &= [\mathrm{T}_\mathrm{c}^\mathrm{C}(A_1(k))\ \ \mathrm{T}_\mathrm{c}^\mathrm{C}(A_2(k))\ \ \cdots\ \ \mathrm{T}_\mathrm{c}^\mathrm{C}(A_n(k))]^\mathrm{T} \end{aligned} \tag{2}$$

In equation (2), $A_i'(k) = \mathrm{T}_\mathrm{c}^\mathrm{C}(A_i(k)) = I_i \times A_i(k)$ is called the clonal of antibody A_i, which show that the antibody realizes the increase of biologic induced by antigen, where $i = 1, 2, \cdots, n$, and I_i is the row vector of element I.

b. **Immune gene operating T_m^C**

The immune gene operating has the crossover and aberrance. Based on the distribution of information exchange diversity characteristics of biological monoclonal antibody and polyclonal antibody, the ICS only adopted aberrance is called monoclonal Selection Algorithm (MCSA), and the ICS adopted crossover and aberrance is called Polyclonal Selection Algorithm (PCSA). Immunology believes that the generation of the affinity maturation and the antibody diversity depend mainly on the high frequency mutation of antibody, not crossover or regroup. In this chapter, we adopt the MCSA only including aberrance and denote the ICS. The individual after mutation is $A''(k) = T_m^C(A'(k))$.

c. **Clone selection operating T_s^C**

Immune selection operator T_s^C indicates the process selecting the optimal individual from the sub-group of antibody after clone and come into being new groups, which denotes as $A(k+1) = T_s^C(A''(k) \cup A(k))$. Therefore, the ICS is described as follows:

$$C_s : A(k) \xrightarrow{\tau_c^C} A'(k) \xrightarrow{\tau_m^C} A''(k) \xrightarrow{\tau_s^C} A(k+1)$$

The ICS enlarges the search range and is helpful to prevent evolution premature and search fall into the local minimum. In other words, the clone is a process changing a low-dimensional space into a higher-dimensional space to solve and mapping the solution into the low-dimensional space.

The basic ICS algorithm is described as the mathematics model of Markov Chain. As the encoding mode is determined, the ICS process likes the random walk with memory from a state to another.

3. Low visible light and infrared image fusion based on the NSCT and the ICS

3.1 Fusion strategy

In this section, we propose the fusion algorithm based on NSCT and the ICS optimization fusion algorithm. We consider the characteristics of coefficients on each multiresolution decomposition level and each subband, and adopt different fusion rules to lowpass subband and detail subbands. Figure 2 illustrates a single analysis/synthesis stage of NSCT processing.

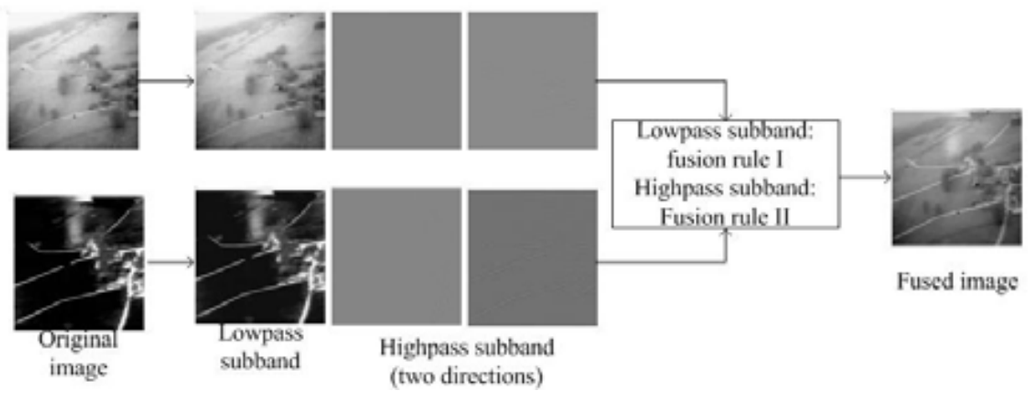

Fig. 2. Image fusion processing based on the one-level NSCT

Because the remote sensing image has no desired contrast image and we expect the image with more detail information and texture information. Therefore, the cost function is defined as the values of the Edge-dependent fusion qualidity index (EFQI) maximax and as the affinity function of ICS. During the process of searching optimization weights, we introduce the elitist preserved definition to keep the weights corresponding to the current best affinity function and save the memory space.

Definition (Elitist preserved) Suppose that $S^* = \{S^* : f(S_l^*) = \min(f(S_l^*)), l = \lg 2(N), \ ,\cdots,2,1\}$ where S_l^*, S_{l-1}^* are the sets (memory population) of optimal directions on l level and $l+1$ level, $f(S_l^*)$ and $f(S_{l-1}^*)$ are the corresponding values of object function. If $f(S_l^*)$, $> f(S_{l-1}^*)$ then $S_l^* := S_{l-1}^*$ and $f(S_l^*) := f(S_{l-1}^*)$.

Without of generalization, we only focus on two source image. There is the same to many source images. Suppose all the source images are registrated, that is, each image being aligned to the same pixel position. If the sensors to be fused are not perfectly aligned, any

corrections to the alignment can be made through a low-latency image warp function. The fusion algorithm is as follows:

Step 1. Loading source images;

Step 2. Performing multi-level NSCT. Suppose that the source images are I_1 and I_2 , we have the approximation sub-band on the last decomposition level and the subimage series of detail sub-band on each decomposition level;

Step 3. Performing the fusion rule of absolute-values maximum to combine corresponding detail sub-band images;

Step 4. Performing the ICS to search the optimal fusion weights to the corresponding approximation sub-images on the last decomposition level adaptively,

$$F_{cA} = \alpha cI_1 + (1-\alpha)cI_2 \tag{3}$$

where cI_1 , cI_2 and F_{cA} denote the approximation subimages of source images I_1 , I_2 and the synthesis image, $\alpha(0 \le \alpha \le 1)$ is the resulting weights. The corresponding ICS sub-algorithm as following and shown in Figure 3:

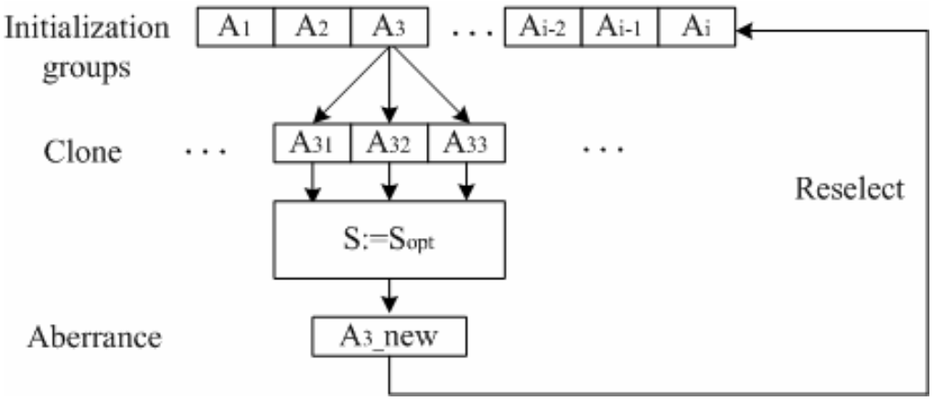

Fig. 3. Block diagram of the clonal selection algorithm

Step 4.1. Initialization. Pre-select the weights in [0, 1] and denoting them initial group individuals with the size of $i = 9$. Let the clone generations is ten.

Step 4.2. Calculating the affinity values of the initial group individuals and storing them in memory cell in sort;

Step 4.3. Clone. Cloning the initial group. Suppose the clone size is three, that is, each individual is cloned to three child individuals by random changes around the father individual. And then we calculating the affinity values of the child individuals;

Step 4.4. Aberrance. Compare the three child individuals with the corresponding father individual, based on an affinity measure. If the affinity value of the child is larger than its father counterpart, then the former replaces the latter and be kept to the memory cell $S := S_{opt}$. Otherwise, the father individual is kept;

Step 4.5. Reselection. Return to step4.3 and repeat the optimization procedure until satisfy the stop condition;

Step 5. Substitute the resulting optimal weights to equation (3) and fusion the appreciation subimages;

Step 6. Performing inverse NSCT to obtain the fused image.

3.2 Experiments and results

Subjective visual perception gives the direct comparison. However, it is easily influenced by Visual Psychological Factors. Therefore, the effect of image fusion must base on subjective vision and combined with objective quantitative valuation criterions. For the remote sensing images, the desired standard image cannot be acquired. Hence, the index such as root mean square error and peak value of signal to noise is unusable. In this section, we adopt the following statistic index to performance the fusion results entirely, such as mean value, standard deviation, entropy, mutual information, cross-entropy, weighted fusion quality index and edge-dependent fusion quality index, et al.

a. **Mean value (MV)**: The MV is the gray mean value of the pixels in a image and the average brightness reflecting to human eye. Suppose the size of the image is MN, $I(i,j)$ is the pixel in the image, then the MV is defined as:

$$MV = \frac{1}{NM}\sum_{i=0}^{N-1}\sum_{j=0}^{M-1} I(i,j) \tag{4}$$

b. **Standard deviation (STD)**: The variance of image reflects the dispersion degree between the gray values and the gray mean value. The STD is the square root of the variance. The large the STD is, the more disperse the gray level. The definition of the STD is:

$$STD = \sqrt{\frac{\sum_{i=0}^{N-1}\sum_{j=0}^{M-1}[I(i,j)-MV]^2}{NM}} \tag{5}$$

c. **Information entropy (IE)**: The IE of the image is an important index to measure the abound degree of the image information. Based on the principle of Shannon information theory, the IE of the image is definition as:

$$E = -\sum_{i=0}^{255} P_i \log_2 P_i \tag{6}$$

where P_i is the ratio of the number of the pixels, which the gray equals to i, and the total number of the pixels. IE reflects the capacity of the information carried by images. The large the IE is, the more information the image carries.

d. **Weighted fusion quality index (WFQI) and Edge-dependent fusion qualidity index (EFQI)**: WFQI and EFQI are evaluation indexes without standard referred image and consider some aspect of the human visual system. Suppose y_A', y_B', y_F' are edge images of the source images y_A, y_B and fused image y_F, respectively. WFQI is introduced to weight feature information of the fused images comes from source images. EFQI focuses on human visual system sensitivity to the edge information. The two measures have a dynamic range of [-1, 1]. The closer the value to 1, the higher the quality of the composite image is.

$$Q_{WFQI}(y_A, y_B, y_F) = \sum_{\omega \in Q} c(\omega)(\rho_A(\omega)Q_0(y_A, y_F, |\omega) + (1-\rho_A(\omega))Q_0(y_B, y_F, |\omega)) \tag{7}$$

$$Q_{EFQI}(y_A, y_B, y_F) = Q_{WFQI}(y_A, y_B, y_F)^{1-\alpha} \cdot Q_{WFQI}(y_A', y_B', y_F')^{\alpha} \tag{8}$$

where $c(\omega) = C(\omega) / [\sum_{\omega \in Q} C(\omega')]$, and $C(\omega) = \max(\eta((y_A \mid \omega), \eta(y_B \mid \omega))$ denotes the overall saliency of a window, $\rho_A(\omega) = \eta(y_A \mid \omega) / (\eta(y_A \mid \omega) + \eta(y_B \mid \omega)), \eta(y_A \mid \omega)$ is some salient features of image y_A in the window ω. In this chapter, we select the energy as the salient feature and the size of the window is 3×3. Q is the summation of the total windows and Q_0 is the general image quality index. The parameter α in equation (8) expresses the contribution of the edges images compared to the original images, and its variation range is [0, 1]. Here we select $\alpha = 0.2$. LOG operator was adopted to obtain the edge image. However, the LOG operator cannot provide the edge directional information and sensitive to noise. Therefore, we select canny operator to detect the edge information, which detect the edges by searching the local maximum of image gradient. Canny operator detects the strong edges and weak edges with the two thresholds, respectively, where the thresholds are system automatic selection. Just when the weak edges and strong edges are jointed and the weak edges may be combined in the output. The canny operator is not sensitive to noise and can detect the true weak edges.

e. **Mutual Information (MI)**: MI of source images A、B and the fused image F is defined:

$$MI((A,B);F) = \sum_{i=0}^{L-1} \sum_{j=0}^{L-1} \sum_{k=0}^{L-1} p_{BAF}(i,j,k) \ln \frac{p_{BAF}(i,j,k)}{p_{BA}(i,j) p_F(k)} \tag{9}$$

where $p_{BAF}(i,j,k)$ is the normalized grey-level histogram of images A, B and F. MI denotes how much the information of fused image extracts from source images. The larger the MI is, the more information the fused image from source images.

f. **Cross-entropy (CE) and Root mean square cross entropy (RCE)**: Let $P = \{p_1, p_2, \cdots, p_i, \cdots, p_m\}$, $Q = \{q_1, q_2, \cdots, q_i, \cdots, q_m\}$, the CE of P and Q is

$$CE(P,Q) = \sum_{i=1}^{m} p_i \ln(p_i / q_i) \tag{10}$$

CE directly reflects the difference of the corresponding pixels between two images. The smaller the CE is, the smaller the difference is. The RCE denotes the comprehensive difference by considering the two CE and denoted as

$$RCE = \sqrt{\frac{CEN_1^{\,2} + CEN_2^{\,2}}{2}} \tag{11}$$

To allow helicopter pilots navigate under poor visibility conditions (such as fog or heavy rain) helicopters are equipped with several imaging sensors, which can be viewed by the pilot in a helmet mounted display. A typical sensor suite includes both a low-light-television (LLTV) sensor and a thermal imaging forward-looking-infrared (FLIR) sensor. In the current configuration, the pilot can choose on of the two sensors to watch in his display. A possible improvement is to combine both imaging sources into a single fused image which contains the relevant image information of both imaging devices.

The two source images are geometric adjustment and with the size of 256×256 . This group images have uniform area, point informatiomn, linear information and texture information. The fusion methods are WT and ICS-based (WT-ICS), CT and ICS (CT-ICS), and NSCT and ICS-based (NSCT-ICS). Without of generality, the decomposition level of the adopted transform is all three. The WT adopts the 9-7 biorthogonal wavelet. The corresponding LP filter banks of CT and NSCT are all adopted 9-7 filter banks obtained from 9-7 1-D prototypes. And the DFB are adopted 'pkva' ladder filters proposed by Phong et al [15], which are with the decomposition 0, 0, 0, 3, 4 corresponding to the five levels LP decomposition, respectively. The decomposition values of DFB correspond to the directions decomposition number, such as "3" denote the direction decomposition number is $2^3 = 8$, and so on.

From the human visual system (as shown in Figure 4), we can see that our fusion technique based on NSCT-ICS is superior to any other fusion methods. The fusion image has the clear edges information, texture information and good definition and contrast than that of based on WT-ICS, NWST-ICS and CT-ICS.

The comparisons of fusion results are shown in Table 1. From the table I, we can see that the quantitative evaluation indexes are in accord with the visual effect. The fusion results based on our proposed adaptive fusion technique are superior to WT-ICS, NSWT-ICS and CT-ICS based fusion methods, which embody in the moderate brightness and the dispersion degree between the gray values, the larger entropy, the larger mutation information, the smaller difference to the source images and the more edge information. From the whole effects, and by virtue of our proposed adaptive fusion technique, the NSCT-based fused result is better than that of the WT-based, nonsubsample wavelet transform-based, and the CT-based, respectively.

Fusion methods	Fusion results						
	MV	STD	IE	WFQI	EFQI	MI	RCE
Visible image	157.75	50.25	5.27	—	—	—	—
Infrared image	41.45	64.55	4.11	—	—	—	—
WT-ICS	162.70	69.09	5.14	0.44	0.39	2.27	2.37
NSWT-ICS	175.14	70.63	4.94	0.55	0.49	2.79	0.34
CT-ICS	162.70	65.12	5.08	0.44	0.39	2.27	4.12
NSCT-ICS	175.14	70.65	4.94	0.56	0.50	2.80	0.32

Table 1. Comparison of the two algorithms by reconstruction precision and runtime

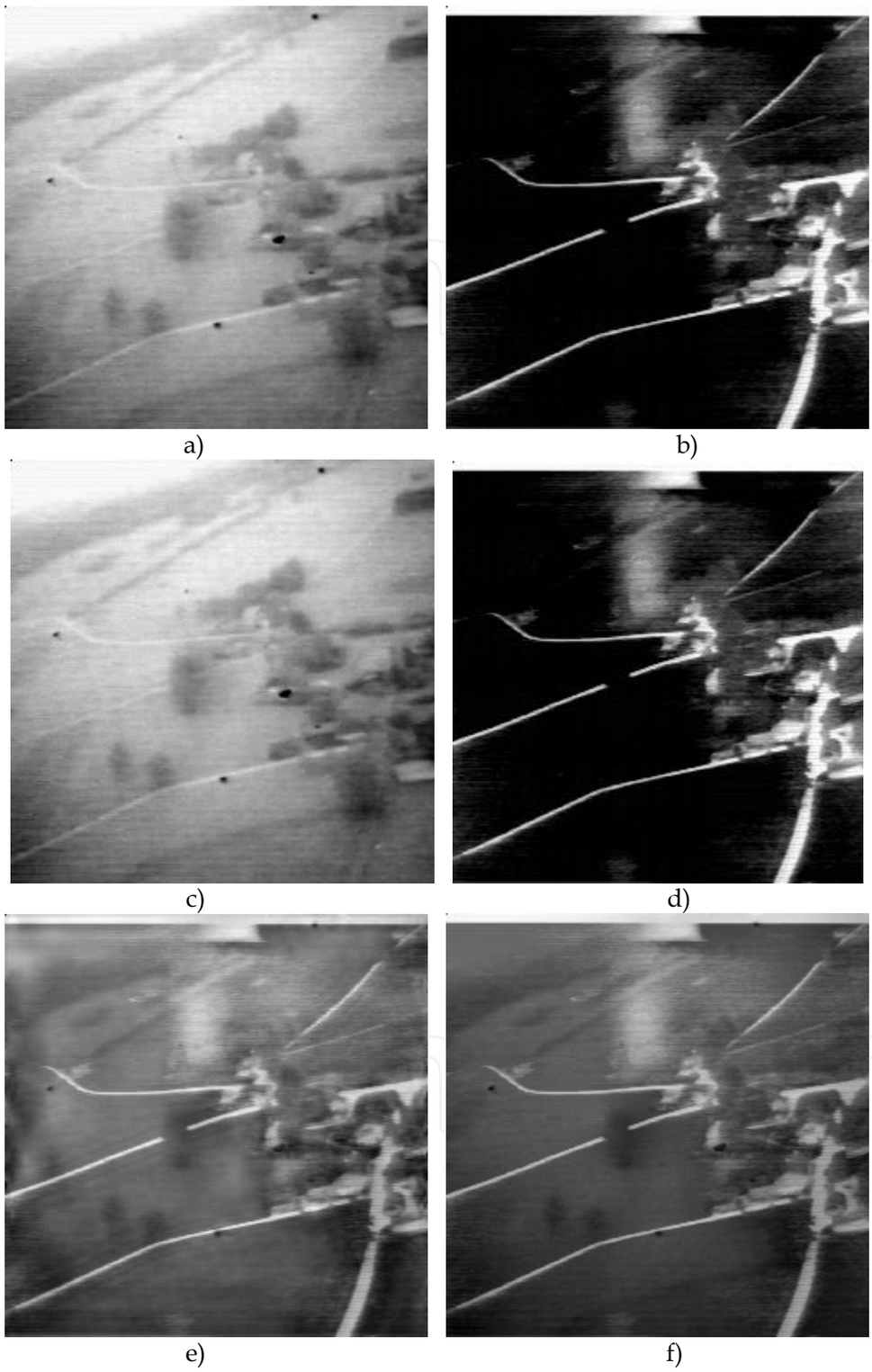

Fig. 4. Compaison of fused images based on different transforms (a) Visible source image (b) Infrared source image (c) WT-ICS based fused image (d) NSWT-ICS based fused image (e) CT-ICS based fused image (f) NSCT-ICS based fused image

4. High resolution and multispectral remote image fusion based on the LHS and the NSCT

4.1 Fusion strategy

In this section, an adaptive panchromatic and multispectral remote sensing image fusion technique is presented based on the NSCT and the LHS transform after analyzing the basic principles of PAN image and MS image and fusion purpose. Here, we adopt an intensity (brightness) component addition method, that is, the detail information of the high-resolution PAN image is added to the corresponding intensity component of the low-resolution image's high frequency subbands to preserve some spectral information.

An image can be represented by RGB color system in computer. However, the RGB color system disagrees with the comprehensive and cognition habits of the human visual system. Human always recognize the color with three features, that is, intensity (I), hue (H), and saturation (S), called IHS system. I component is decided by the spectral main wave length and denotes the nature distintion. S component symbolizes the proportion of the main wave length of the intensity. I component means the brightness of the spectral. In the IHS space, spectral information is mostly reflected on the hue and the saturation. From the visual system, we can conclude that the intensity change has little effect on the spectral information and is easy to deal with.

For the fusion of the high-resolution and multispectral remote sensing images, . the goal is ensuring the spectral information and adding the detail information of high spatial resolution, therefore, the fusion is even more adequate for treatment in IHS space.

IHS color space transform means the change of image from RGB space components to IHS spatial information I component and spectral information H and S components. However, the general IHS color system has the disadvantage that neglects two components when computing the brightness values. The IHS system results in that the brightness of pure color is the same as the achromatic color. Therefore, we adopt the LHS color system to solve the paoblem. The LHS color system generates the brightness with the value of 255 to achromatic color pixel and the value of 85 to pure color pixel.

The detailed process of this fusion algorithm is as follows:

Step 1. Perform polynomial interpolation to keep the edges of the linear landmark and make the PAN and SPOT images with the same sizes.

Step 2. Transform the RGB representation of the multispectral image by LHS transformation into the intensity, hue, and saturation(L. H. S)components.

$$L = \frac{r+g+b}{3} \tag{12}$$

$$S = 1 - 3 \times \frac{\min(r,g,b)}{r+g+b} \tag{13}$$

$$H = \frac{arc\cos\{0.5 \times [(r-g)+(r-b)]\}}{\sqrt{(r-g)^2+(r-b)(g-b)}} \tag{14}$$

The corresponding matrix expression is as follows

$$\begin{bmatrix} I \\ v_1 \\ v_2 \end{bmatrix} = \begin{bmatrix} 1/3 & 1/3 & 1/3 \\ 1/\sqrt{6} & 1/\sqrt{6} & -2/\sqrt{6} \\ 1/\sqrt{2} & -1/\sqrt{2} & 0 \end{bmatrix} \begin{bmatrix} R \\ G \\ B \end{bmatrix} \tag{15}$$

$$H = \tan^{-1}(\frac{v_1}{v_2}) \tag{16}$$

$$S = \sqrt{v_1^2 + v_2^2} \tag{17}$$

Step 3. Apply histogram matching between the original panchromatic image and multispectral intensity component to get new panchromatic high-resolution(PAN HR) image and multispectral intensity(MSI) component image.

Step 4. Decompose the matched MSI image and PAN HR image to get the NSTC decomposition coefficients.

Step 5. Fuse the detail and approximate coefficients of the MSI and PAN HR according to (25)and(26), respectively.

$$Fuse_{low} = MSI_{low} \tag{18}$$

$$Fuse_{high} = \sum MSI_{\det ails} + \sum PANHR_{\det ails} \tag{19}$$

Step 6. Apply the inverse NSCT transform to the fused detail and approximate coefficients to reconstruct the new intensity component I_{new}

Step 7. Perform the inverse LHS transform to the new intensity component, new I, together with the hue and saturation components to obtain the fused RGB images.

$$\begin{bmatrix} R \\ G \\ B \end{bmatrix} = \begin{bmatrix} 1 & 1/\sqrt{6} & 1/\sqrt{2} \\ 1 & 1/\sqrt{6} & -1/\sqrt{2} \\ 1 & -2/\sqrt{6} & 0 \end{bmatrix} \begin{bmatrix} I \\ v_1 \\ v_2 \end{bmatrix} \tag{20}$$

4.2 Experiments and results

The test source images are the SPOT PAN image and LANDSAT TM5, 4, 3 bands image of the same area. The TM image was acquired on February 17, 1993, and the SPOT PAN images were obtained on May 28, 1995. The two source images were after geometric adjustment and with the size of 256×256.

The fusion methods are traditional PCA and IHS, WT-based weighted fusion(WT-W), WT and LHS transform-based(WT-LHS), CT and LHS transform-based(CT-LHS), NSCT and LHS transform-based (NSCT-LHS). Without loss of generality, the decomposition levels of the adopted transforms are all three. The WT adopts the 9-7biorthogonal wavelet. The corresponding LP filter banks of CT and NSCT are all adopted 9-7 filter banks obtained from 9-7 1-D prototypes. And the DFB are adoped "pkva" ladder filters proposed by phong et al., which are with the decomposition 0, 3, 4 corresponding to the three levels of LP decomposition, respectively. The fusion results are shown in Fig. 5.

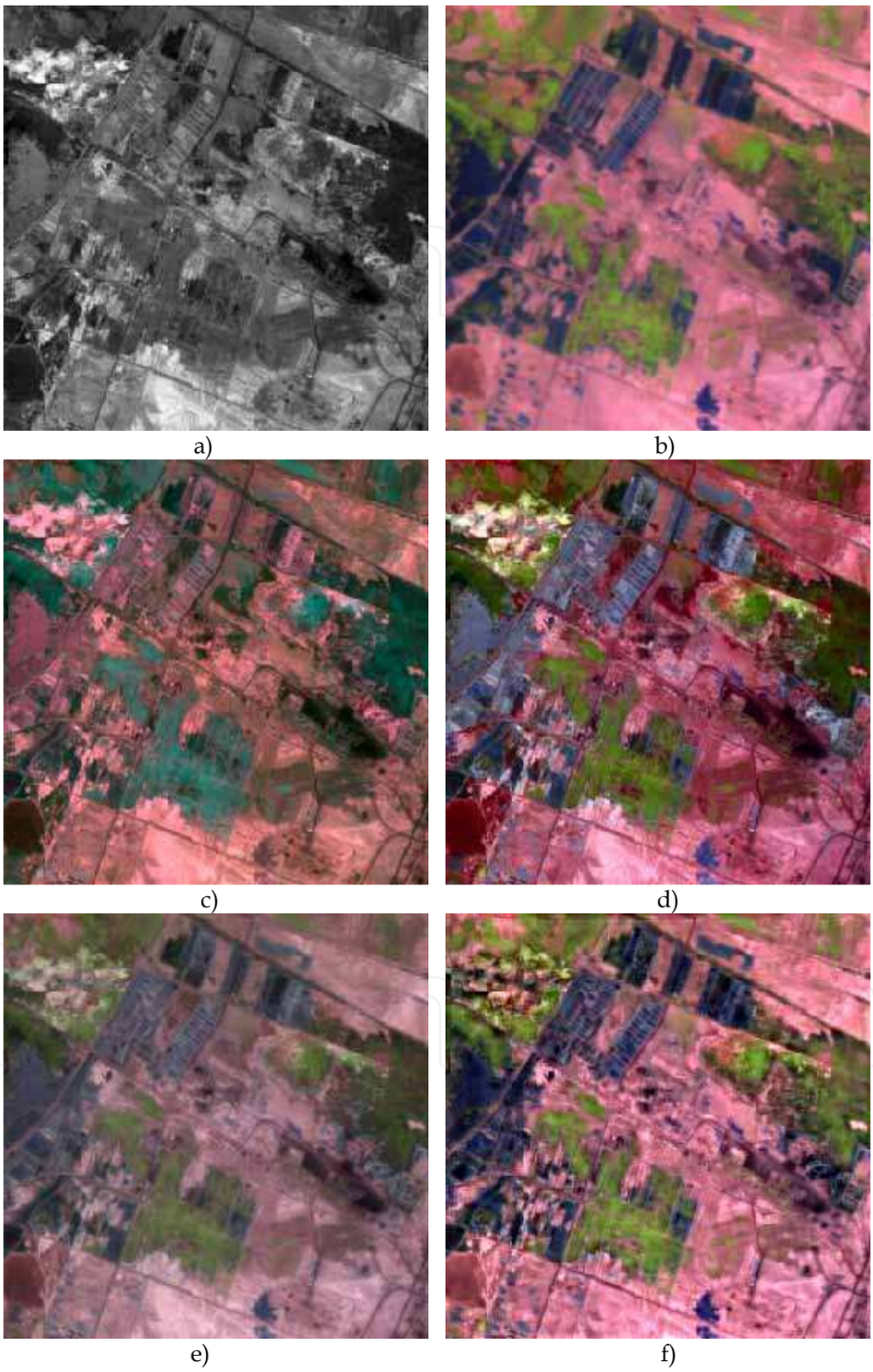

a) b)

c) d)

e) f)

g) h)

Fig. 5. (a) SPOT image (b) TM image (c) PCA fusion image (d) IHS fusion image (e)WT-W fusion image (f) WT-LHS fusion image (g) CT-LHS fusion image (h)NSCT-LHS fusion image

From the human visual system, we can see that our fusion technique based on the NSCT-LHS can improve spatial resolution and at the same time hold spectral information well. Our intensity added fusion technique based on LHS transform is superior to classical PCA fusion method and IHS transform fusion method, and the WT-W fusion method. The fused image has more information of the source images, which is demonstrated in spatial resolution, definition, micro-detail difference, and contrast. The adaptive intensity component addition method preserves the whole spatial information, which has the advantage of the utilization of the detail information of the two source images. The fusion method only uses high-resolution information to adjust intensity component and better holds the multispectral information and texture information and introduces the high-resolution characteristic in multispectral image. Moreover, the fusion algorithm based on NSCT-LHS has more outstanding detail information than those based on WT-LHS and CT-LHS.

In this section, we adopt the following statistic index to performance the fusion results entirely, such as mean value, standard deviation, information entropy, weighted fusion quality index, average gradient, correlation coefficient, bias index, spectrum distoration and et al.

a. **Average gradient(AG)**:AG is the index to reflect the expression ability of the little detail contrast and texture variation, and the definition of the image. The calculation formula is

$$g = \frac{1}{(M-1)(N-1)} \sum_{i=1}^{(M-1)(N-1)} \sqrt{[(\frac{\partial f}{\partial x})^2 + (\frac{\partial f}{\partial y})^2]/2} \tag{21}$$

Generically, the larger g, the more the hierarchy, and the more definite the fused image.

b. **Correlation coefficient(CC)**:The CC denotes the degree of correlation of two images. The more the CC close to 1, the higher the correlation degree is. The definition is denoted as

$$corr(\frac{A}{B}) = \frac{\sum_{j=1}^{n}\sum_{i=1}^{m}(x_{i,j} - \mu(A))(x'_{i,j} - \mu(B))}{\sqrt{\sum_{j=1}^{n}\sum_{i=1}^{m}(x_{i,j} - \mu(A))^2 (x'_{i,j} - \mu(B))^2}} \tag{22}$$

where A and B are two images, $x_{i,j}$ and $x'_{i,j}$ denote the pixels of A and B, respectively, $\mu(A)$ and $\mu(B)$ are the corresponding mean values of the two images.

c. **Spectrum distortion (SD)**: SD means the distortion degree of a multispectral image and is defined as follows:

$$W = \frac{1}{M \times N}\sum_{j=1}^{N}\sum_{i=1}^{M}|I_f(i,j) - I(i,j)| \tag{24}$$

where I(i, j) and If(i, j) are the pixels of the source and fused images, respectively. The larger value of W, the higher the distortion.

d. **Bias index**: This is an index of the deviation degree between fused image and low-resolution multispectral image:

$$Bias = \frac{1}{M \times N}\sum_{i=1}^{M}\sum_{j=1}^{N}\frac{|I_f(i,j) - I(i,j)|}{I(i,j)} \tag{25}$$

From Table 2, we can see that the quantitative evaluation indexes are in accord with the visual effect. The fusion results based on our adaptive fusion technique are superior to the traditional PCA and IHS fusion methods, which embody the moderate brightness and the dispersion degree between the gray values, the larger entropy , the stronger correlation degree. From the whole effects, and by virtue of our proposed adaptive fusion technique, the NSCT-based fused results are better than those of the WT-based, and the CT-based, respectively, especially for the spectral holding. The better values are underlined.

The comparison of the histogram images of R, G, B components of the TM multispectral images and the NSCT-based fusion image are shown in Figure 6, respectively.

From the comparison of the R, G, and B components histograms, we can conclude that the dynamic range of fused image is larger than that of the source image, that is , the fused image has more detail information and higher special resolution than that of the source image.

Fusion methods	MV	STD	IE	AG	CC	SD	Bias	Q_w	Q_E
SPOT PAN	92.45	9.55	7. 30	12.75	-	-	-	-	-
TM	102.82	47.68	4.96	9.50	-	-	-	-	-
PCA	94.08	46.62	5.08	18.74	0.52	58.40	0.58	0.53	0.51
IHS	92.45	80.80	5.24	13.85	0.66	38.24	0.36	0.52	0.50
WT-W	102.88	37.55	5.00	8.86	0.85	32.23	0.27	0.52	0.43
WT-LHS	112.66	54.37	5.33	16.21	0.92	14.79	0.14	0.51	0.44
CT-LHS	112.66	53.23	5.31	16.80	0.92	15.02	0.14	0.52	0.45
NSCT-LHS	112.72	52.66	5.30	16.76	0.93	14. 22	0.13	0.54	0.47

Table 2. Comparison of fusion results

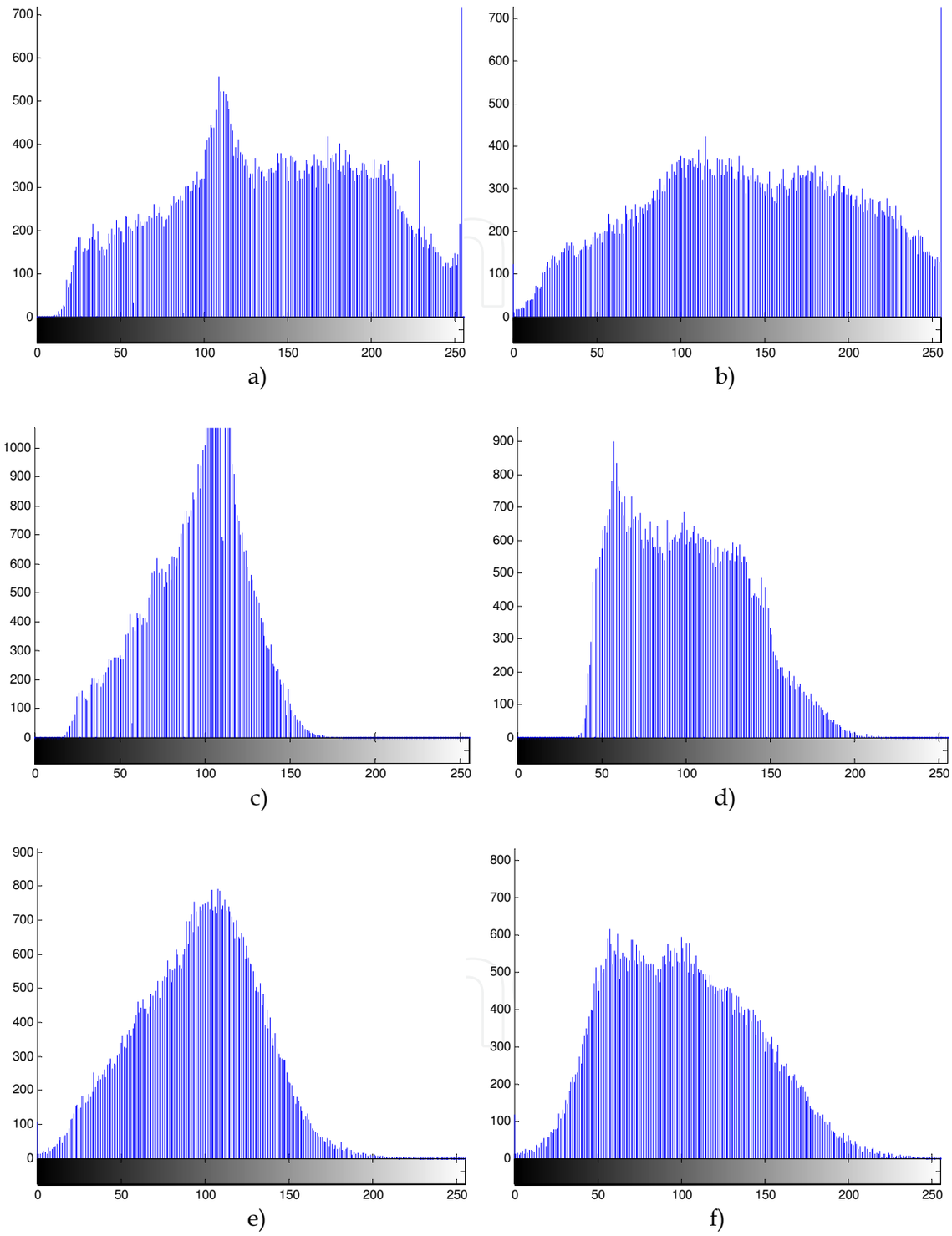

Fig. 6. The R, G, and B components histograms of TM source image and the NSCT-LHS fusion image (a)R component of TM source image (b)R component of NSCT-LHS fusion image (c)G component of TM source image (d) G component of NSCT-LHS fusion image (e)B component of TM source image (f) B component of NSCT-LHS fusion image

5. Multisensor image fusion based on the CP and MW-HMT

5.1 CP decomposition and HMT model

The construction of CP structure is as follows (A. Toet 1990): Firstly, a Gaussian pyramid is constructed. This is a sequence of images in which each image is lowpass filtered and subsampling copy of its predecessor. We denote original images as $I(i,j), i \le m, j \le n$, when m and n are the number of row and column of images, respectively. Let G_l present the level l of the Gaussian pyramid decomposition and array G_0 contains the original image. This array G_0 becomes the bottom or zero level of the pyramid structure. Each node of pyramid level l ($1 \le l \le N$, where N is the index of the top level of the pyramid) is obtained as a Gaussian weighted average of the nodes at level $l-1$ that are positioned within a 5×5 window centered on that node. Convolving an image with a Gaussian-like weighting function is equivalent to applying a lowpass filter to the image. Gaussian pyramid construction generates a set of lowpass-filtered copies of the input image, each with a bandlimit one octave lower than that of its predecessor. Because of the reduction in spatial frequency content, each image in the sequence can be represented by an array that is half as large as that of its predecessor in both directions. The process that generates each image in the sequence from its predecessor is called REDUCE operation since both the sampling density and the resolution are decreased. Thus, for $1 \le l \le N$ we have

$$\begin{aligned} G_l &= REDUCE(G_{l-1}) \\ G_l &= \sum_{m=-2}^{2} \sum_{n=-2}^{2} w(m,n) G_{l-1}(2i+m, 2j+n), 0 < l \le N, 0 \le i < C_l, 0 \le j < R_l. \end{aligned} \tag{26}$$

where N is the total levels of the pyramid, C_l and R_l are the number of column and row of the level l, respectively, and $w(m,n)$ is a weighted function, which satisfies some conditions. We can choose the weighting function:

$$w = \frac{1}{256} \begin{bmatrix} 1 & 4 & 6 & 4 & 1 \\ 4 & 16 & 24 & 16 & 4 \\ 16 & 24 & 36 & 24 & 6 \\ 4 & 16 & 24 & 16 & 4 \\ 1 & 4 & 6 & 4 & 1 \end{bmatrix} \tag{27}$$

CP analysis scheme is based on local luminance contrast. This scheme computes the ratio of the lowpass images at successive levels of the Gaussian pyramid. Since these levels differ in sample density, it is necessary to interpolate new values between the given values of the lower frequency image before it can divide the higher frequency image. Interpolation can be achieved simply by defining the EXPAND operation as the inverse of the REDUCE operation.

Let $G_{l,k}$ be the image obtained by applying EXPAND to G_l k times. Then

$$\left.\begin{aligned} G_{l,0} &= G_l \\ G_{l,k} &= EXPAND(G_{l,k-1}) \end{aligned}\right\} \tag{28}$$

meaning

$$G_{l,k}(i,j) = 4\sum_{m=-2}^{2}\sum_{n=-2}^{2} w(m,n)G_{l,k-1}(\frac{i+m}{2},\frac{j+n}{2}) \tag{29}$$

where only integer coordinates $(\frac{i+m}{2},\frac{j+n}{2})$ contribute to the sum. A sequence of ratio images R_i is defined by

$$\left.\begin{array}{c} R_i = \dfrac{G_i}{EXPAND(G_{i+1})}, for\ 0 \le i \le N-1 \\ R_N = G_N \end{array}\right\} \tag{30}$$

Thus, every level R_i is a ratio of two successive levels in the Gaussian pyramid.
Luminance is defined as

$$C = (L - L_b)/L_b = L/L_b - I \tag{31}$$

where L denotes the luminance at a certain location in the image plane, and L_b represents the luminance of the local background, and I is the unit gray image, that is I(i,j)=1 , for all i,j . When C_i is defined as

$$\begin{array}{c} C_i = \dfrac{G_i}{Expand(G_{i+1})} - I \quad 0 \le \mathrm{i} \le \mathrm{N} \\ \mathrm{C}_N = G_N \end{array} \tag{32}$$

Combining with formula (36), we have

$$R_i = C_i + I \tag{33}$$

Therefore, we refer to the sequence as CP. G_0 can be recovered exactly by reversing the above steps as formula (40)

$$\left.\begin{array}{l} G_N = R_N \\ G_i = (C_i + I)Expand(G_{i+1}) = R_i Expand(G_{i=1}) \qquad 0 \le i \le N-1 \end{array}\right\} \tag{34}$$

Hidden Markov models (M. S. Crouse, 1998) can capture the correlation of multiscale of images effectively, it is a very practical operation and the probability model can depict coefficient between the statistical characteristics of joint effectively. Figure 7 shows a multiwavelets hidden markov tree(HMT) model for one subhand. We model each coefficient(black node) as a Gaussian mixture controlled by a hidden state variable(white node). To capture the persistence across scale property of multiwavelets (Salesnick, I. 1998), we connect the states vertically across scale in Markov-1 chains. We agreed on the following: an indicator of the quadtree between different nodes, the root node, the coefficient of mw1

shall state for S1, p(i) represent the parent node of i. We do the following description for this model.

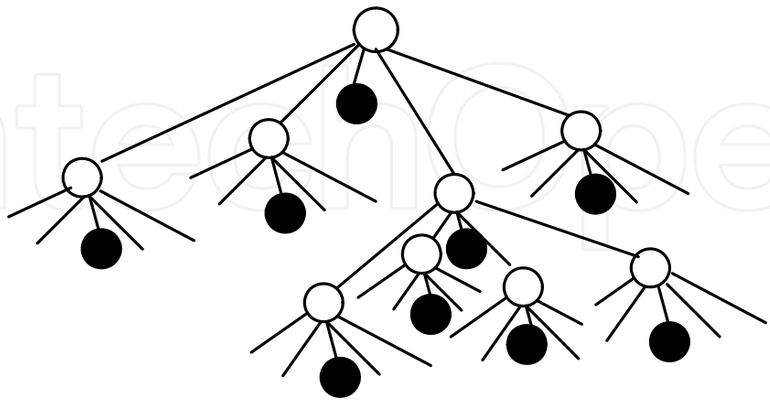

Fig. 7. Multiwavelets coefficient and HMT modle for one subband

5.2 Fusion strategy

a. Iterated Algorithm Based CP and GHM

Step 1. Initialization. Suppose the number of CP decomposition level is 4. The two original; images to be fused are denoted as "m_1" and "m_2", respectively;

Step 2. CP decomposition. According to the number of decomposition level pre-supposed;

Step 3. decompose each original image using window function and obtain two images with size of $(N/2^4)\times(N/2^4)$ denoted as "M_1" and "M_2", respectively.

b. The iterative algorithm combining with HMT model

Step 1. Initialize: Set the initial model to estimate for θ 0, and set l =0;

Step 2. E step. Train the two multiwavelets M1' and M2' separately, which got from step 3 of algorithm 3.3. Calculate each child coefficient P(S | mw, θ l), which is the weighting function of the state probability, and the maximum value of $E_S\left[\ln f(\mathrm{mw},S|\theta)\middle|\mathrm{mw},\theta^l\right]$;

Step 3. M step. Updata $\theta^{l+1}=\arg\max_\theta E_S\left[\ln f\left(\mathrm{mw},S|\theta\right)\middle|\mathrm{mw},\theta^l\right]$;

Step 4. Set the constringency threshold for 10^{-5}. Iterative can be termination, when two iterative convergence error is less than 10^{-5}. Establishment HMT model for the last $l=l+1$, and can get two group train coefficient $c1$ and $c2$;

Step 5. According to the modulus maxima of fusion rules, get new coefficient c by taking coefficients corresponding maxima modulus position $c1$ and $c2$.

c. Iterated Algorithm Combining with ICS Optimizing

Step 1. Initialization. Taking the coefficient matrix obtained from step 5 in above algorithm as the original population $A(0)$, in which each element can be regarded as chromosome. The original number of generation is k=1, and the maximal number of iterated generation G_S=20;

Step 2. Terminating condition judgment. Judge whether the terminating condition is satisfied or not. That is, if the pre-supposed times of iteration is finished, stop and determine the current population composed by current individual as the optimized solution population and turn to step 8; else turn to step 3;
Step 3. Clone operation. Clone operation is performed to the *k*-th generation parent population A (k) to obtain A'(k);
Step 4. Mutation operation. Gaussian mutation with square error 0.1 is performed to A′(k) to obtain A″(k) ;
Step 5. Affinity function computation;
Step 6. Clonal selection operation. In child population, if exist muted antibody $b = \max\left\{a_{ij} \middle| j = 2,3,...,q_i - 1\right\}$ making $Q(a_i) < Q(b)$, $a_i \in A(k)$, then choose b to enter the new parent population;
Step 7. k=k+1, turn to step 2;
Step 8. Obtaining a group of optimized fusion coefficients denoted as "result-coefficient" and reconstruction in light of this group of coefficients;
Step 9. CP reconstruction according to the parameter "result-coefficient" from step 8;
Step 10. Output the final fusion result;

5.5 Experiments and results

The test source images are two bands of mutisensor images. The fusion methods are traditional and multiwavelet transform. Without loss of generality, the decomposition levels of the adopted transforms are all three. The WT adopts the "db8" wavelet. The fusion results are shown in Fig. 8 and Fig. 9. In the experiments, Fig.8 (a), (b) and Fig.9 (a), (b) are satellite images of two different sensor respectively.
From the visual effect, the resulting images fused by WT-based method (Fig.8(c) and Fig. 9(c)), MWT-based method (Fig.8(d) and Fig. 9(d)) are fairly well, but our proposed method (Fig.8 (e) and Fig.9 (e)) is more clear and contains structural details, which contain richer structure content and spatial information and reconstruct the interesting targets. In a word, compared with the results of the fusion obtained by the other techniques, the results of the ICS-CPMWHMT fusion have better visual effect.
In addition to visual analysis, we conducted a quantitative analysis. We based our analysis of the experimental results on the many factors; namely, the information entropy (IE), the average grads (AG) and the standard deviation (STD). Using these factors such as IE, AG and STD, Table 3 to Table 4 compares the experimental results of image fusion for the ICS-CPMWHMT method and the other methods.
IE refers to the change of information capability. The more the information included in the image, the better the fused image. AG can reflect the capability to represent the detail contrast of images sensitively and can be used to assess the definition of images. STD is an index to measure the contrast value of images. But for the fusion of infrared and visual image, if IE value is too high, maybe over smooth the image; if STD value is too high, maybe lose too much spectral information. So when we assess fused image using these factors, combine with visual effect in general.
IE value of the fused image by ICS-CPMWHMT method keeps at a high level. AG value and STD value of fused images are also moderate, which show that fused images not only reflect the detail features also retain plenty detail information better. It is benefit and significant for following target automatic recognition and classification.

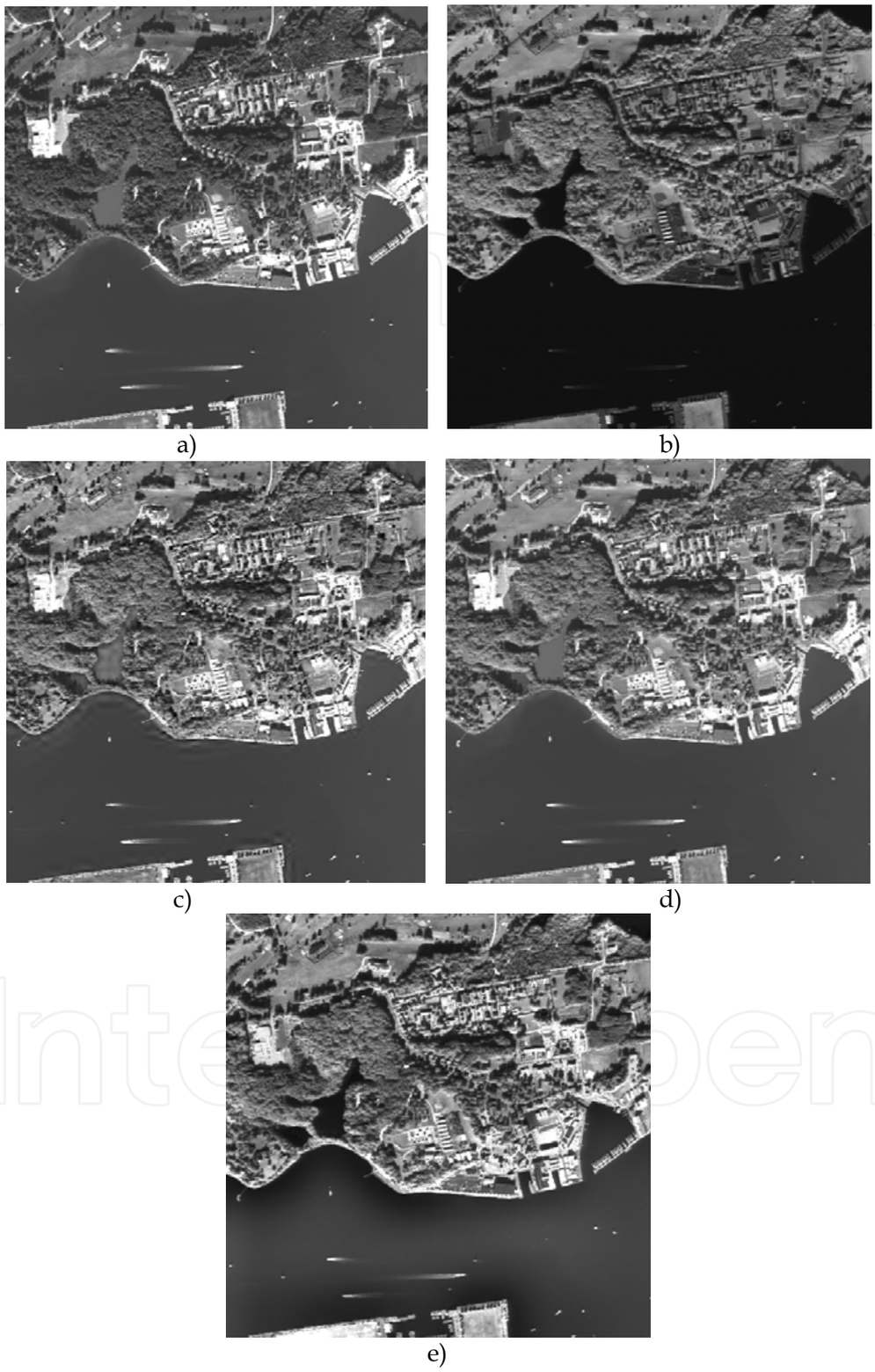

a) b) c) d) e)

Fig. 8. (a) The image of sensor 1 (b) the image of sensor 2 (c) WT fusion image (d) MWT fusion image (e) ICS-CPMWHMT fusion image

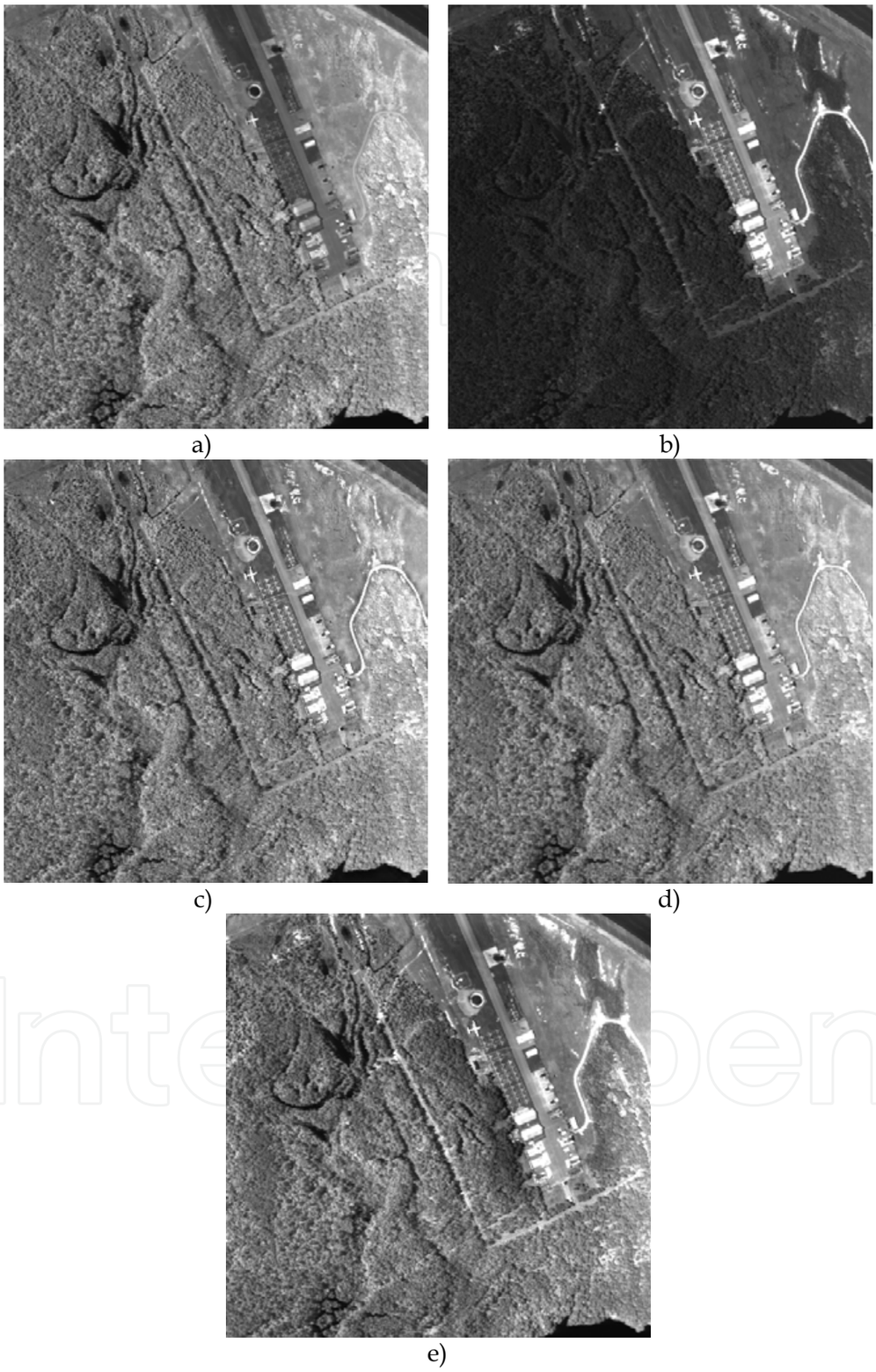

Fig. 9. (a) The image of sensor 1 (b) The image of sensor 2 (c) WT fusion image (d) MWT fusion image (e) ICS-CPMWHMT fusion image

Image 1	IE	AG	STD
Sensor 1	4.59	9.92	48.80
Sensor 2	4.10	8.43	50.00
WT	4.82	12.35	52.22
MWT	4.76	11.56	51.71
ICS-CPMWHMT	5.08	13.30	61.71

Table 3. Comparison of fusion performance on image 1

Image 2	IE	AG	STD
Sensor 1	5.13	12.23	41.96
Sensor 2	4.63	6.08	39.09
WT	4.93	13.30	43.64
MWT	5.13	11.95	42.47
ICS-CPMWHMT	5.13	14.86	50.14

Table 4. Comparison of fusion performance on image 2

6. Conclusion

The multiscale geometry analysis tool and ICS algorithm are adopted to three remote sensing images fusion in this chapter, including the multi-sensor images, the lower spatial resolution multispectral image and the higher spatial resolution panchromatic image, the infrared image and visible light image.

Fristly, we propose a panchromatic high-resolution image and multispectral image fusion technique, which is based on NSCT and LHS transform. We take full advantage of the NSCT, including good multiresolution,shift-invariance, and multidirectional decomposition. And an intensity compenent addition technique is introduced into the NSCT domain to better improve the spatial resolution and hold the spectral information and texture information,simultaneously. Experiments that the proposed fusion technique is more effective than other traditional fusion methods and has some improvements,especially for holding of spectral information,texture information,and contour information.

Secondly, based on NSCT and ICS strategy, we take full advantage of the NSCT with the good shift-invariance and multi-directional decomposition. And the ICS in introduced into the NSCT domain to optimize the fusion weights adaptively. From quantitative analysis, we can hold the conclusion that our fusion technique can take full advantage of the low light image and infrared image and have improvements both in vision and in quantitative index.

From the subjectivity and objectivity, we can conclusion that our proposed fusion technique is more effective than other traditional fusion methods and has improvements, especially for the holding of more clear texture and contour information. Experiments show that the proposed fusion technique is a preferred and effective remote sensing image fusion method.
Thirdly, based on multiwavelet-domain HMT models and ICS optimization, we explain a novel intelligence optimization technique. The immune clonal selection technique is introduced into image fusion to obtain the optimal fusion weights adaptively. Experimental results show that the proposed approach has improvements in visual fidelity and quantitative analysis.
Finally, in the ICS algorithm optimizing fusion coefficients, iterative times need to be preinitialized or experientially selected; also it decides the runtime of whole the technique. So it is our further work to study self-adaptive ICS algorithm to apply in the fusion processing. How to solve the fusion problem of remote images without desired compared images is our future work.

7. References

A. Toet (1990). Hierarchical image fusion, *Machine Vision and Applications*, Vol. 3, No. 1, (1999) pp. 1-11, 19900932-8092

da Cunha, A. L.; Jianping Zhou & Do, M. N. (2006). The nonsubsampled contourlet transform: theory,design and applications, *IEEE Transactions on Image Processing*, Vol. 15, No.10, (Oct. 2006) pp.3089-3101, 3089-3101

De Castro, L. N., Von Zuben, F. J.(2000). The Clonal Selection Algorithm with Engineering Applications. Procedings of GECCO'00, Workshop on Artificial Immune Systems and Their Applications. (July 2000) pp. 36-37, Las Vegas, USA

Do, M. N. & Vetterli, M. (2005). The contourlet transform:an efficient directional multiresolution image representation, *IEEE Transactions on Image Processing*, Vol. 14, No. 12, (Dec. 2005) pp. 2091-2106, 2091-2106

Gonzalez-Audicana. M.; Saleta, J. L.; Catalan, R. G. & Garcia, R. (2004). Fusion of multispectral and panchromatic images using improved HIS and PCA mergers based on wavelet decomposition, *IEEE Transactions on Geoscience and Remote Sensing*, Vol. 42, No. 6, (June 2004) pp. 1291-1299, 0196-2892

Jianping, Zhou; Cunha, A. L. & Do, M. N. (2005). Nonsubsampled contourlet transform: construction and application in enhancement, *Proceedings of IEEE International Conference on Image Processing*, pp.469-472, 0-7803-9134-9, 11-14 Sept. 2005, Dept. of Electr. & Comput. Eng., Illinois Univ., Champaign, IL, USA

M. S. Crouse, R. D. Nowak, R. G. Baraniuk (1998). Wavelet-based statistical signal processing using hidden Markov models. *IEEE Transactions on Signal Processing*, (Apr 1998), Vol. 46, No. 4, pp. 886-902, 1053-587X

Nunez, J.; Otazu, X.; Fors, O.; Prades, A.; Pala,V.&Arbiol,R. (1999). Multiresolution-based image fusion with additive wavelet decomposition, *IEEE Transaction on Geoscience and Remote Sensing*, Vol. 37, No.3, (May 1999) pp.1204-1211, 0196-2892

Rockinger, O. (1996). Pixel-level fusion of image aequences using wavelet frames, *Proceedings of Image Fusion and Shape Variability Techniques*. pp. 149-154, July 3-5, UK:Leeds University Press, Leeds

Salesnick, I. (1998). Multiwavelet bases with extra approximation properties. *IEEE Transactions on Signal Processing*, Vol. 46, No. 11, (Nov 1998) pp. 2898-2908, 1053-587X.

Wang, Z. J.; Ziou, D.; Armenakis, C.; Li, D. & Li, Q. G. (2005). A comparative analysis of image fusion methods, *IEEE Transactions on Geoscience and Remote Sensing*, Vol. 43, No. 6, (June 2005) pp.1391-1402, 0196-2892

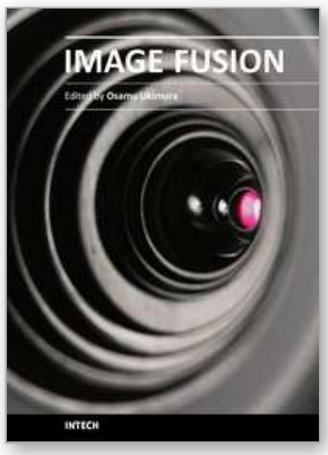

Image Fusion
Edited by Osamu Ukimura

ISBN 978-953-307-679-9
Hard cover, 428 pages
Publisher InTech
Published online 12, January, 2011
Published in print edition January, 2011

Image fusion technology has successfully contributed to various fields such as medical diagnosis and navigation, surveillance systems, remote sensing, digital cameras, military applications, computer vision, etc. Image fusion aims to generate a fused single image which contains more precise reliable visualization of the objects than any source image of them. This book presents various recent advances in research and development in the field of image fusion. It has been created through the diligence and creativity of some of the most accomplished experts in various fields.

How to reference
In order to correctly reference this scholarly work, feel free to copy and paste the following:

Fang Liu, Jing Bai, Shuang Wang, Biao Hou and Licheng Jiao (2011). Image Fusion Based on Multi-Directional Multiscale Analysis and Immune Optimization, Image Fusion, Osamu Ukimura (Ed.), ISBN: 978-953-307-679-9, InTech, Available from: http://www.intechopen.com/books/image-fusion/image-fusion-based-on-multi-directional-multiscale-analysis-and-immune-optimization

INTECH
open science | open minds

InTech Europe
University Campus STeP Ri
Slavka Krautzeka 83/A
51000 Rijeka, Croatia
Phone: +385 (51) 770 447
Fax: +385 (51) 686 166
www.intechopen.com

InTech China
Unit 405, Office Block, Hotel Equatorial Shanghai
No.65, Yan An Road (West), Shanghai, 200040, China
中国上海市延安西路65号上海国际贵都大饭店办公楼405单元
Phone: +86-21-62489820
Fax: +86-21-62489821

IntechOpen